Published in final edited form as:
*J Chem Phys*. 2011 July 14; 135(2): 024502. doi:10.1063/1.3601750.

# Collective translational motions and cage relaxations in molecular ionic liquids

**Christian Schröder**
University of Vienna, Department of Computational Biological Chemistry, A-1090 Austria

## Abstract

In this computational study, the collective translational motions of 1-ethyl-3-methylimidazolium triflate, characterized by its current correlation function and its collective dipolar displacement, are interpreted in terms of an ion cage around a central ion. Thereby, a coincidence of the relevant time constants is observed. Furthermore, the ion cage is long living and its composition is rather heterogeneous. Besides high numbers of counter ions, several ions of like charge populate the first shell around a central ion. In contrast to the strong influence of the local environment on the collective translational motion, rotations are strictly collective. In other words, a local picture falls short of describing the overall antiparallel alignment of ionic dipoles.

A further issue of this work is the interpretation of the initial region of the collective dipolar displacement. It can be related to all collective translational processes showing up in the computational dielectric spectrum. In particular, slow translational processes which are invisible in the current correlation function can be detected. The inclusion of these slow processes allow for an excellent computational reconstruction of the experimental spectrum of the generalized dielectric constant.

## I Introduction

### Molecular ionic liquids are a fascinating class of soft matter

These organic salts typically consist of imidazolium based cations with weakly basic anions and combine the characteristics from charged and dipolar species on the very same molecule.[1–3] Because of their hybrid nature, a single molecular ion can contribute to the translation of charges as well as to the rotation of dipoles thus combining the properties of ionic melts and neutral molecular liquids. Focusing on their ionic character one would expect a translational ordering resembling that of a crystalline structure. Indeed, one observes a typical charge ordering[4–7], i.e. a sequence of charge layers of alternating sign[8–12]. But ionic liquids are more than a mere liquid salt. Their observed translational and rotational dynamics, however, contrasts with the picture of a quasi-crystalline system since a pronounced molecular mobility is found[13,14]. Consequently, there must exist forces which counteract these strong electrostatic forces causing charge ordering. Obviously, the steric and electronic anisotropy of cations (and to a minor degree of anions) as well as their difference in size and shape are an important sources of counteraction.[15]

The hybrid character of the molecular ions can also be visualized on a mesoscopic level in computational dielectric spectroscopy.[1] The transport of charges is characterized by the


Europe PMC Funders Author Manuscripts

dielectric conductivity $\vartheta(\omega)$ whereas the rotational and intramolecular motions contributes to the dielectric permittivity $\epsilon(\omega)$. While experiments can only provide the sum of these two components, the so-called generalized dielectric constant $\Sigma^*(\omega)$, computational studies can evaluate $\vartheta(\omega)$ and $\epsilon(\omega)$ separately.[16–21] The decomposition of the generalized dielectric constant into dielectric conductivity and permittivity corresponds to a split up of the total collective dipole moment into its translational and ro-vibronic collective dipole moments. Although these collective dipole moments are uniquely defined,[22] some problems due to periodic boundary conditions occur when computing the collective translational dipole: Molecules which leave the simulation box during the simulation period are reinserted at the opposite side in order to keep the number of molecules in the simulation box constant. This poses no problems for the non-translational collective dipole moment but causes huge jumps in the translational dipole moment. One remedy to cope with this discontinuity is the a *posteriori* unfolding of the simulation data yielding a so-called "itinerant dipole moment".[23,24] Alternatively, one may derive the dielectric conductivity from the collective current which is continuous because ionic velocities are conserved when crossing the box surface. The benefits or drawbacks of both methods will be a central issue of the present study.

A second issue is the high collectivity of ionic motion, i.e. translational motion of ions in an ionic liquid cannot be understood as the migration of an ensemble of *single independent* ions. If this would be so, the diffusion coefficients of the larger imidazolium cations should be much lower than those of the smaller anions, e.g. triflate, which is not the case.[25–27] Therefore, the translational motion of ions must be coupled in some sense to their environment. Another evidence of this coupling is visible in the Δ-parameter of the Nernst-Einstein equation of the static conductivity:

$$\sigma_{\mathrm{NE}}(0) = \frac{\rho q^2}{k_B T}(D_+ + D_-)(1 - \Delta) \tag{1}$$

The coupling parameter Δ *does not describe* the ratio of ion pairs to single ions, but the reduction of the conductivity due to the collective interactions of all cations and anions with *all other cations and anions.* Of course, long-lived individual ion pairs — should they be present in the sample – will contribute to Δ. The values of Δ have a large range from roughly 0.1 to 0.9 in molecular ionic liquids.[1] This shows on the one hand the uniqueness of each cation-anion combination. On the other hand, the interactions of some compositions of molecular ionic liquids seem to have a *very strong collective* character.

In diluted ionic solutions the central ion will be surrounded by a "cloud" of ions of the opposite charge. Two effects will reduce the conductivity of the sample: First, the "relaxation effect" or "asymmetry effect" is the rebuilding of the ion clouds when cations and anions are accelerated in opposite directions by the electric field.[28] As a result, the center-of-mass of the ion cloud lags behind the center-of-mass of the central ion. Second, the "electrophoretic effect" is caused by the additional friction due to the opposite direction of the velocities of the central ion and its ion cloud. A simple description of this situation is the well-known Debye-Hückel theory with a spherical ion cloud and an uniform dielectric

constant.[28–30] However, in a pure molecular ionic liquid the situation is more complex. The solution is not dilute. Consequently, the local environment cannot be represented by a continuum with an uniform dielectric constant. [31] Since the cations are anisotropic (thus having a non-spherical first shell) the ion cage must be anisotropic, too. Therefore, traditional shell models with their inherent sphericity based on radial distribution function cannot be applied. Distance based-shells, however, are plagued by the introduction of a large set of parameters which have to be calibrated for the specific situation. Therefore, we will apply a general parameter-free concept of ion cage which is based on the Voronoi tessellation of space.[32–35]

Of course, the central ion reacts to distortions or relaxations of the cage. In traditional force field models this “reaction” was restricted to translation and ro-vibronic motion. However, the central ion can also respond to the local environment by a reorganization of its charge distribution. At the electronic level this would be a rather complicated procedure[36–40] but it can be mimicked by the inclusion of polarization forces.[41,42] Furthermore, it turned out that many body polarization forces accelerate the ion dynamics and thus bring computational dynamics closer to the experimental one. [25,26,43–45]

## II Methods

A detailed description of the simulation is given in Ref. 26 and 46. Therefore, we give only a brief summary here: We simulated 1000 polarizable 1-ethyl-3-methyl-imidazolium triflate ($EMIM^+CF_3SO_3^-$) in a cubic box with a box length of 67.195Å under periodic boundary conditions for a simulation period of 35 ns with a time step of 0.5 fs. The classical force field parameters stemmed from Ref. 47–49. The permanent partial charges $q_{i\beta}$ of $EMIM^+$ were changed to the values reported in Ref. 50 in order to better reproduce the experimental viscosity.[17,20,21] The polarization of the atoms was modeled by the so-called “Drude oscillators”: Here, mobile Drude particles were bound by a harmonic spring with a force constant $k_{i\beta}^{\delta}$ to their reference atoms

$$k_{i\beta}^{\delta} = \frac{1}{4\pi \in_0} \cdot \frac{\left(q^{\delta}\right)^2}{2\alpha_{i\beta}} \tag{2}$$

and carried in our case a charge $q^{\delta}$ of -1.0 e. They had an uniform mass of $m^{\delta} = 0.1$ amu which was subtracted of the mass of the corresponding atom.[51,52] The atomic polarizabilities $\alpha_{i\beta}$ of the non-hydrogen atoms were taken from Ref. 53 and hydrogens were left unpolarizable. It was shown in Ref. 46 that these polarizabilities resulted in a reasonable high frequency limit $\epsilon_\infty$=1.94 which is in close proximity to the experimental value of 2.3. The induced dipole moment $\boldsymbol{\mu}_{i\beta}^{ind}$ of the atom $i\beta$ equals the distance vector $\mathbf{d}_{i\beta}$ between the mobile Drude particle and its reference atom times the Drude charge $q^{\delta}$.

The interactions between permanent charges $q_{i\beta}$ and Drude pairs were excluded betweenatoms which shared a bond or an angle.[54] The interaction between the corresponding Drude pairs were screened by an exponential Thole function with a radius of 1.3 Å according to Ref. 54. The Drude particles were thermostatted at 1 K with a

Europe PMC Funders Author Manuscripts

relaxation time constant of 5 fs.[55] All non-Drude particles were thermostatted at 300 K by a Nose-Hoover thermostat with a relaxation time constant of 100 fs. In Ref. 26 we have shown that these Drude parameters ensure the proximity of the Lagrangian method to self-consistency.

Nonbonded and image lists were updated heuristically using a 16 Å neighbour list distance. Lennard-Jones energies and forces were smoothly switched off between 11 and 12 Å. The electrostatic forces of both, Drude particles and the attached atoms, are treated by the PME technique.[56,57] The "cutoff" for the real-space part interactions was 12 Å and the damping constant for the reciprocal-space interactions is 0.410 $Å^{-1}$. The grid spacing equals 1.05 Å and a sixth-order spline interpolation of the charge to the grid was used.

## III Theory

Exposing an overall neutral sample to a spatially homogeneous, external electric field of harmonic frequency ω induces a dielectric polarization $\mathbf{P}(\omega)$. In case of a small-amplitude electric fields the dielectric polarization $\mathbf{P}(\omega)$

$$\mathbf{P}(\omega) = \frac{\Sigma^*(\omega)}{4\pi}\mathbf{E}(\omega) \tag{3}$$

scales with the internal Maxwell electric field E(ω) which counteracts the external field. The susceptibility $\Sigma^*(\omega)$ is called "generalized dielectric constant" (GDC) and can be computed from equilibrium simulations of polarizable systems by

$$\Sigma^*(\omega) = \frac{4\pi}{3V}\frac{1}{k_B T}\mathscr{L}\left[-\frac{d}{dt}\langle \mathbf{M}_{tot}(0)\cdot\mathbf{M}_{tot}(t)\rangle\right] + \frac{4\pi}{3V}\mathrm{tr}\langle\mathscr{A}\rangle\,. \tag{4}$$

The macroscopic polarizability tensor $\mathscr{A}$ represents the electronic degrees of freedom causing a high-frequency limit of $4\pi\,\mathrm{tr}\langle\mathscr{A}\rangle/3V = \epsilon_\infty - 1$.[26,58] The frequency-dependent part of the GDC is made up by the Fourier-Laplace transform of the negative time derivative of the auto-correlation function of the total collective dipole moment $\mathbf{M}tot(t)$. It is defined by

$$\mathbf{M}_{tot}(t) = \sum_i \sum_\beta \left(q_{i\beta}\cdot\mathbf{r}_{i\beta} + \boldsymbol{\mu}_{i\beta}^{ind}\right) \tag{5}$$

$$= \mathbf{M}_D^{perm}(t) + \mathbf{M}_J(t) + \mathbf{M}_D^{ind}(t) \tag{6}$$

The summation runs over all atoms $\beta$ of all molecules $i$. The sum of all induced atomic dipoles $\boldsymbol{\mu}_{i\beta}^{ind}$ result in a collective induced dipole moment $\mathbf{M}_D^{ind}(t)$ which shows similar time behavior as the collective ro-vibrational dipole moment $\mathbf{M}_D^{perm}(t)$.[26] The computation of both properties from trajectory data of an molecular dynamics simulation is straight forward. Since their auto-correlation functions behave similar in time, one may unite both collective

dipole moments $\mathbf{M}_D^{ind}(t)$ and $\mathbf{M}_D^{perm}(t)$ to the non-translational collective dipole moment $\mathbf{M}_D(t)$.

## A Collective translation in a toroidal system

Unfortunately, the collective translational dipole moment $\mathbf{M}_J(t)$ causes problems and prohibits a direct computation of the total collective dipole moment $\mathbf{M}_{tot}(t)$ and its auto-correlation function. Since molecular dynamics simulations are subject to periodic boundary conditions, $\mathbf{M}_J(t)$ suffers from toroidal jumps of charged molecules $i$ from one side of the box to the other. Neutral molecules do not cause problems since they are not contributing to $\mathbf{M}_J(t)$. Since we are practically interested in large ensembles of cations and anions, the simulation box size $L$ is very large, so the jump $q_i$. $L$ experienced by $\mathbf{M}_J(t)$ due to the toroidal shift is large as well. In principle, there are two possibilities to circumvent this problem:

First, The jump of a charged molecule $i$ changes its coordinates and thus the center-of-mass $\mathbf{r}_i$ but its center-of-mass velocity $\mathbf{v}_i$ remains unchanged. Hence, the collective current $\mathbf{J}(t) = \sum_i qi \cdot \mathbf{v}_i = d\mathbf{M}_J(t)/dt$ is not plagued with toroidal jumps. As a result, the Fourier-Laplace transform in Eq. (4) may be reformulated in terms of $\mathrm{J}(t)$ and $\mathrm{M}_D(t)$

$$\mathscr{L}\left[-\frac{d}{dt}\langle \mathbf{M}_{tot}(0)\cdot\mathbf{M}_{tot}(t)\rangle\right] = \left\langle \mathbf{M}_D^2\right\rangle + i\omega\mathscr{L}[\langle \mathbf{M}_D(0)\cdot\mathbf{M}_D(t)\rangle] - 2\mathscr{L}[\langle \mathbf{M}_D(0)\cdot\mathbf{J}(t)\rangle] + \frac{i}{\omega}\mathscr{L}[\langle \mathbf{J}(0)\cdot\mathbf{J}(t)\rangle] \tag{7}$$

using $-d^2/dt^2\langle \mathbf{M}_J(0)\cdot\mathbf{M}_J(t)\rangle = \langle \mathbf{J}(0)\cdot\mathbf{J}(t)\rangle$.[1,21] The last equation also elucidates the traditional interpretation of the GDC, i.e. its splitting into a dielectric permittivity

$$\in(\omega) - \in_\infty = \frac{4\pi}{3Vk_BT}\left(\left\langle \mathbf{M}_D^2\right\rangle + i\omega\mathscr{L}[\langle \mathbf{M}_D(0)\cdot\mathbf{M}_D(t)\rangle] - \mathscr{L}[\langle \mathbf{M}_D(0)\cdot\mathbf{J}(t)\rangle]\right) \tag{8}$$

and dielectric conductivity

$$\vartheta(\omega) = \frac{4\pi i}{3Vk_BT_\omega}([\mathscr{L}\langle \mathbf{J}(0)\cdot\mathbf{J}(t)\rangle] + i\omega\mathscr{L}[\langle \mathbf{M}_D(0)\cdot\mathbf{J}(t)\rangle]) = \frac{4\pi i}{\omega}\sigma(\omega)\,. \tag{9}$$

The cross term $\langle \mathbf{J}(0)\cdot\mathbf{J}(t)\rangle$ contributes marginally and can thus be neglected for practical purposes.[16] Therefore, the conductivity $\sigma(\omega)$ is given by

$$\sigma(\omega) \simeq \frac{\mathscr{L}[\langle \mathbf{J}(0)\cdot\mathbf{J}(t)\rangle]}{3Vk_BT}\,. \tag{10}$$

The current correlation function $\langle \mathbf{J}(0)\cdot\mathbf{J}(t)\rangle$ can be represented by a sum of damped oscillator functions




Europe PMC Funders Author Manuscripts

$$f_{\mathrm{JJ}}(t) = \sum_k A_k \cos(\omega_k t + \delta_k)\exp(-t/\mathscr{T}_k) \tag{11}$$

which can be easily Fourier-Laplace transformed.[21] However, $f_{\mathrm{JJ}}(t)$ may also be used to calculate the static conductivity $\sigma(0) = \lim_{t\to\infty} \sigma_J(t)$. The running integral $\sigma_{\mathrm{j}}(t)$ is given by

$$\sigma_J(t) = \frac{1}{3Vk_BT}\int_0^t \langle \mathbf{J}(0)\cdot\mathbf{J}(t')\rangle dt' . \tag{12}$$

Because of the exponential character of the fit function only the lower limit of this integral contributes to the static conductivity. Furthermore, $\sigma_{\mathrm{j}}(t)$ obtained from the numerical integration of $\langle \mathbf{J}(0)\cdot\mathbf{J}(t)\rangle$ can be used to detect translational relaxation processes with time constants $T_k$ of a few picoseconds which are not directly visible in $\langle \mathbf{J}(0)\cdot\mathbf{J}(t)\rangle$.[20] Relaxation processes at longer times cannot be extracted from $\sigma_{\mathrm{j}}(t)$ due to its noisy character in these time regimes. Therefore, one has to look for alternative ways to detect these processes.

The second possibility to avoid the jumps affecting $\mathbf{M}_{\mathrm{J}}(t)$ is the unfolding of the trajectory post simulation. In other words, during the simulation the molecules which pass a boundary of the simulation box are reinserted at the opposite side of the box due to the periodic boundary condition. For the analysis, however, these reinsertions are undone, i.e. the molecules translate outside the original box. As a result, this unfolded $\mathbf{M}_{\mathrm{J}}(t)$ has no jumps and is called "itinerant dipole moment" in literature.[23,24] However, it increases with time as the charged molecules depart more and more from the original box. This implies that the auto-correlation function $\langle \mathbf{M}_J(0)\cdot\mathbf{M}_J(t)\rangle$ of the unfolded $\mathbf{M}_{\mathrm{J}}(t)$ depends on the length of the simulation trajectory. In other words, the complete $\langle \mathbf{M}_J(0)\cdot\mathbf{M}_J(t)\rangle$ is shifted upwards with increasing length of the trajectory.[1]

This drift in absolute values can be removed by considering the relative quantity $\Delta\mathbf{M}_J(t) = \mathbf{M}_J(t) - \mathbf{M}_J(0)$. As shown in Ref. 16 its mean-squared displacement is related to the current by

$$\left\langle \Delta\mathbf{M}_J^2(t)\right\rangle = 2\left(\mathrm{t}\int_0^t \langle \mathbf{J}(0)\cdot\mathbf{J}(t')\rangle dt' - \int_0^t t'\langle \mathbf{J}(0)\cdot\mathbf{J}(t')\rangle dt'\right) \tag{13}$$

$$= 2\left(t\cdot 3\,V\,k_BT\sigma_J(t) - \int_0^t t'\langle \mathbf{J}(0)\cdot\mathbf{J}(t')\rangle dt'\right) \tag{14}$$




Europe PMC Funders Author Manuscripts

In the asymptotic limit the second term approaches the constant $\left\langle \mathbf{M}_J^2 \right\rangle = -\int_0^\infty t' \langle \mathbf{J}(0) \cdot \mathbf{J}(t') \rangle dt'$ while the first term becomes a linear function

$$\lim_{t >> t_c} \left\langle \Delta \mathbf{M}_J^2(t) \right\rangle = 6\, V\, k_B T \sigma(0) t + 2 \left\langle \mathbf{M}_J^2 \right\rangle \tag{15}$$

after the correlation length $t_c$ is reached. In other words, $t_c$ is that time beyond which the integral in Eq. (12) reaches a plateau value, the static conductivity $\sigma(0)$. On the one hand the last equation is frequently used to compute $\sigma(0)$.[16–18,20,59–61] This "Einstein-Helfand" relation is to be preferred to "Green-Kubo" equation (12).[62,63] On the other hand, it demonstrates that the relative $\Delta \mathbf{M}_J(t)$ leads to a constant, bound value of $\left\langle \mathbf{M}_J^2 \right\rangle$ although it is computed from the unfolded $\mathbf{M}_J(t)$ which increases with time.

So far, our focus was on the asymptotic behavior of $\left\langle \Delta \mathbf{M}_J^2(t) \right\rangle$ which is essentially a linear function for $t \gg t_c$. For shorter times the behavior is much more complex. One way of characterization is the study of their derivatives: The first derivative of $\left\langle \Delta \mathbf{M}_J^2(t) \right\rangle$ with respect to time is given by

$$\frac{d}{dt} \left\langle \Delta \mathbf{M}_J^2(t) \right\rangle = 6\, V\, k_B T \sigma_J(t) \tag{16}$$

showing the equivalence with the running integral of the conductivity in Eq. (12). Therefore, all translational processes which can be detected by $\sigma_J(t)$ can also be found in $\left\langle \Delta \mathbf{M}_J^2(t) \right\rangle$. Additional processes in the transition region ($t \simeq t_c$) can be extracted from $\left\langle \Delta \mathbf{M}_J^2(t) \right\rangle$. In order to convert all these processes to components of a dielectric spectrum the second derivative

$$\frac{d^2}{dt^2} \left\langle \Delta \mathbf{M}_J^2(t) \right\rangle = 2 \langle \mathbf{J}(0) \cdot \mathbf{J}(t) \rangle \,. \tag{17}$$

serves as a link. The last equation can also be easily deduced from the second derivative of Eq. (13). The fit of $\left\langle \Delta \mathbf{M}_J^2(t) \right\rangle$ can thus be converted to contributions of the currentcorrelation function. From the considerations above an appropriate fit function may look like

$$f_{\Delta \mathrm{MJ}^2}(t) = \left( \sum_k \tilde{A}_k \cdot e^{-t/\mathcal{T}_k} - \tilde{A}_k \right) + \tilde{\sigma} \cdot t \,. \tag{18}$$

The slope $\tilde{\sigma}$ of the last term divided by $6VkT$ yields the static conductivity and the negative sum of $\tilde{A}_k$ gives $2\left\langle \mathbf{M}_J^2 \right\rangle$. The corresponding amplitudes $A_k$ for $\langle \mathbf{J}(0) \cdot \mathbf{J}(t) \rangle$ are $\tilde{A}_k / 2\mathcal{T}_k^2$. As a result, slow relaxing, translational processes have very small amplitudes A**k** and are consequently *invisible in a plot* of $\langle \mathbf{J}(0) \cdot \mathbf{J}(t) \rangle$ *but not in a plot* of $\left\langle \Delta \mathbf{M}_J^2(t) \right\rangle$. Having

collected the complete set of translational parameters (including the slow processes), the $\vartheta(\omega)$-spectrum is finally computed by Eq. (9). At zero frequency a static external field induces a current in a sample composed of charged species. In order to eliminate this effect, experimental and computational dielectric spectra are corrected for this conductance.

$$\vartheta_0(\omega) = 4\pi i \frac{\sigma(\omega) - \sigma(0)}{\omega} \tag{19}$$

At the level of our fit function of $f_{\Delta \mathrm{MJ}}{}^2(t)$ this corresponds to a neglect of the last term.

## B Cage resolved collective translational motion

Translational motion of ions is strongly coupled to their environment. The strongest coupling of an ion will be to its next neighbors, i.e. its cage. Although the intuitive picture of an ion cage is very attractive for interpretation, cage dynamics is not easy to rationalize. One way is the concept of a residence function $n_i^j(t)$ of molecules $i$ around a central ion $j$:

$$n_i^j(t) = \begin{cases} 1, & i \in \text{first shell of j at time } t \\ 0, & \text{otherwise} \end{cases} \tag{20}$$

Since re-occurence of molecule $i$ at a later time is not recognized as the entrance of a new particle, the molecular identity $i$ is conserved. The average measure of residence is given by the correlation function $C_i^j(t) = \sum_i \left\langle n_i^j(0) \cdot n_i^j(t) \right\rangle$. The summation may be restricted to a subset of molecules, e.g. all anions. In order to extract the characteristic residence times from $C_i^j(t)$ one can use a multi-exponential fit

$$f_{\mathrm{nn}}(t) = n_\infty + \sum_k \tilde{n}_k \cdot e^{-t/\mathcal{T}_k} \tag{21}$$

for its representation. The mean residence times is then given by $\langle \mathcal{T} \rangle = \sum_k \tilde{n}_k \mathcal{T}_k / \sum_k \tilde{n}_k$. $n_\infty$ represents the “steady state” value of $C_i^j(t)$ and should not be mixed up with the coordination number $\left\langle \mathrm{CN}_i^j \right\rangle$ which is defined by the initial value of the correlation function, $C_i^j(0)$:

$$\mathrm{CN}_i^j = \sum_i \left\langle \left( n_i^j(0) \right)^2 \right\rangle. \tag{22}$$

Here, $j$ and $i$ denote the reference species and species the surrounding molecules, respectively.

The concepts presented so far all depend on the definition of the first shell. Traditionally, shells are constructed as concentric spheres around a reference particle. The coordination number is then computed as the integral over the radial distribution function up to its first




Europe PMC Funders Author Manuscripts

minimum. This poses two classical problems: First, the integration limit differs for each *ij*-combination. Second, and even more critical is the anisotropy of the central molecule. In order to account for this anisotropy one could introduce a shell thickness, i.e. a typical distance of atoms of the counter ions to selected atoms at the surface of the solute. This would introduce a lot of parameters and arbitrary selections. A parameter-free approach to determine direct neighbors is the Voronoi tessellation used in this work.[32–35] It creates space-filling disjunct polyhedra, each containing all space closer to its associated atom than to any other atom. For the interpretation, the atomic polyhedra were merged to molecular polyhedra. If two molecular polyhedra share a face, the corresponding molecules are direct neighbors.

## IV Results And Discussion

Collective translational behavior of an ionic liquid is characterized by its current $J(t)$ which is the time derivative of the collective translational dipole moment $\mathbf{M}_J(t)$. The current auto-correlation function $\langle \mathbf{J}(0) \cdot \mathbf{J}(t) \rangle$ of an ionic liquid shows a strong oscillatory behavior which seems to be totally damped within the first few picoseconds.[5,16,20,63,64]

### A Current correlation function

In case of $EMIM^+CF_3SO_3^-$ the current correlation function $\langle \mathbf{J}(0) \cdot \mathbf{J}(t) \rangle$ is given in Fig. 1a (gray solid line). It can be represented by $f_{JJ}(t)$ with three components $k = 1, 2, 3$ and the parameters given in Table I: The first component ($k = 1$) describes the oscillatory behavior of the current correlation function at very short times which may be associated with the cage vibrations of the molecular ions. The frequency of this vibration $\omega_1 = 17.732$ $ps^{-1}$ corresponds to $\tilde{\nu} = 94$ $cm^{-1}$ which agrees nicely with experimental FIR spectra of imidazolium based ionic liquids showing peaks at frequencies between 62101 $cm^{-1}$.[65,66] This vibration has an oscillations period $T_1 = 1/\omega_1 = 0.056$ ps and reaches its relaxation time $\tau_1 = 0.123$ ps within two oscillation periods. The high frequency $\omega_1$ show the local character of this oscillations, while the strong damping can only be explained as a collective effect, i.e. a strong cage of several neighbors. Anyway, this effect cannot be attributed to an intermolecular vibration with a single counter ion since these kind of vibrations should be much less damped.[66] The oscillation period of the second component $k = 2$ (black dashed line in Fig. 1a) is approximately 20 ps as compared with the relaxation time $\tau_2$ of roughly 0.2 ps. This ratio of two orders of magnitude prohibits the formation of a full oscillation. As a result, the second component appears more as a function with a shallow minimum than an oscillatory motion. As we will see later on, this component may be associated with ultra-fast motions of the cage. At first sight, the two components discussed so far seem to reproduce the current correlation function $\langle \mathbf{J}(0) \cdot \mathbf{J}(t) \rangle$ in Fig. 1a. First doubts arise when computing the static conductivity $\sigma(0)$ on the basis of these two components:[20] Fig. 1b compares the running integral of the conductivity $\sigma_J(t)$ derived from the two component fit (black dash-dotted line) and obtained by numerical integration.[20,62,67] In fact, the asymptotic value $\sigma(0) = 3.6$ S/m of the two fit components is by an order of magnitude larger than the numerical value of 0.75 S/m. The gap between the black dash-dotted line and the numerical gray line can be closed by a third $k = 3$-component with zero frequency and zero phase shift (c.f. Table I). Taking into account all three *k*-components one obtains the black dotted line in

Fig. 1b. However, the third *k*-component (black solid line) is almost invisible in the current correlation function in Fig. 1a. This is a first indication of the problems discussed already in the Theory section when working solely with the current correlation function.

It is interesting to compare the contributions of the fit components $\sigma_k(0)$ to the static conductivity $\sigma_k(0) = \sum_k \sigma_k(0)$ which are given by

$$\sigma_k(0) = \frac{A_k \mathcal{T}_k}{3V k_B T} \frac{\cos(\delta_k) - \mathcal{T}_k \omega_k \sin(\delta_k)}{1 + \mathcal{T}_k^2 \omega_k^2}. \tag{23}$$

For $k = 1, 2, 3$ one gets $\sigma_k(0)$ = 25.56S/m, -21.97S/mand-2.84 S/m, respectively. The sum of these three contributions yields $\sigma(0)$ = 0.75 S/m. The very large contribution of the first component is almost completely compensated by the other two components. Unfortunately, the three detected processes may represent $\sigma_J(t)$ in the first six picoseconds as visible in Fig. 1b but fail to reproduce the long-term limit which is approximately 20% of 0.75 S/m. This fact indicates that there are additional processes which cannot be properly determined by $\langle \mathbf{J}(0) \cdot \mathbf{J}(t) \rangle$ or $\sigma_J(t)$. The time constant of this additional process ($k = 4$) is in the range of 50 to 200 picoseconds. Furthermore, to be honest, $\sigma_k(0)$ in Eq. (23) strongly depends on the time constants $\tau_k$. In particular, in case of $\delta_2 \simeq \pi/2$ and the large amplitude $A_2$ small variations of $\tau_3$ significantly changes the value of $\sigma_2(0)$ and consequently $\sigma(0)$. Altogether, the computation of the static conductivity $\sigma_2(0)$ on the basis of $\langle \mathbf{J}(0) \cdot \mathbf{J}(t) \rangle$ or $\sigma_J(t)$ is an intricate procedure. However, as shown below, more reliable results, especially for the slow modes, can be gained from the collective dipolar displacement.

## B Relaxation of the ionic cage

From a chemist point of view, the first k = 1 component may be seen as the conductive motion of the central ions which is hampered by the lag of their surrounding ion cage. Hence, the second and third component should be related to the ion cloud, i.e. the cage. A typical ion cloud around $EMIM^+$ is shown in Fig. 2. For clarity's sake the hydrogens of the surrounding cations and the oxygens and fluorines of $CF3SO_3^-$ are not displayed.

In contrast to the intuitive view that the cation is surrounded by a cage of anions, the higher number of neighboring cations is interesting. The location of the cationic neighbors is not restricted to the side chain of the central cation; they also approach the imidazolium ring. The anions are very often found in close proximity to the three acidic hydrogens of the cationic imidazolium ring. However, the coordination is *not strictly monovalent* as demonstrated by the two triflates around the H2 of $EMIM^+$ in Fig. 2. A further striking feature of the cage is the alternating sequence of cations and anions. This could be explained by the fact that the repulsion between two like ions is suppressed by an intercalated counter ion.

Fig. 3 shows the anionic cage which occupies less space compared to the cationic cage. Furthermore, the number of counter ions is now higher with a typical ratio of approximately 2:1 and probably due to a highly concentrated negative charge as compared to the more diffusive cationic charge distribution. In other words, the anionic cage is essentially

determined by electrostatic interactions while in the cationic cage steric effects play a role, too.

These pictures are significant snapshots of the local environment around a selected cation and anion. In order to draw quantitative conclusions of the cationic and anionic cages from *all ions* and from *the whole trajectory* one may apply the parameter-free Voronoi method to detect the cages. As a first result, the distribution of cage members $\mathrm{CN}_i^j$, i.e. the mutual coordination numbers, for different combination of ion types can be obtained and are displayed in Fig. 4. The first remarkable result is that the central ions $\mathrm{EMIM}^+$ j have more direct cationic neighbors (black dotted distribution) than triflate (gray solid line). This may be due to the larger surface of $\mathrm{EMIM}^+$ compared to $\mathrm{CF_3SO_3^-}$ which offers more “docking places”. The distribution of coordination numbers between like charges is broadened. Here, the mutual orientation of both ions is of greater concern. The attraction between unlike charges narrows the width of the respective distribution.

The rough balance of cationic and anionic members around a central $\mathrm{EMIM}^+$ and the 2:1 ratio of cations and anions around $\mathrm{CF_3SO_3^-}$ can also be conducted from the average coordination number $\left\langle \mathrm{CN}_i^j \right\rangle$ in Fig. 4. Another fact to mention is that all coordination numbers $\left\langle \mathrm{CN}_i^j \right\rangle$ are very high. For example, each triflate anion has direct contact to eight $\mathrm{EMIM}^+$ on average which makes the classification of “ion pairs” a little bit dubious. Even more, *each hydrogen* of the imidazolium ring have almost always direct contact to *at least one triflate* during the whole simulation period which was also found by Kohanoff *et al.*[36] Comparable high coordination numbers are found for other ionic liquids as well.[9,37] These two references also show the difficulties in determining coordination numbers from radial distribution functions. Ref. 9 stated two different coordination numbers for cation–cation, anion–anion and cation-anion depending on the distance criterion of the shell. Ref. 37 depicted a coordination number as function of the distance to the central ion without specifying the first shell criterion explicitly. The difficulties in determining coordination numbers become even worse when considering anisotropic, non-spherical ions, e.g. imidazoliums with larger side chains. The Voronoi method does not suffer from these problems: The determination of the direct neighbors is done without a “shell parameter” and solely due to contacts of molecules.[33] Consequently, the Voronoi shells are not spherical but adapt to the anisotropic shape of the reference molecules.

Based on the findings of the cage structure the dynamics of the cage may be characterized by the auto-correlation of the residence function $\left\langle n_i^j(0) \cdot n_i^j(t) \right\rangle$ displayed in Fig. 5. Together with the inset which zooms the subpicosecond and picosecond range these correlation functions are found to cover three time regimes: subpicoseconds, a few picoseconds and several nanoseconds. The fit function $f_{\mathrm{nn}}(t)$ of Eq. (21) offers the possibility to quantify these time regimes. The resulting parameters are given in Table II and the corresponding fit as gray lines in Fig. 5. Within the time window shown, the asymptotic value, $n_\infty \simeq 2$, shows that two of eight neighbors of the central ion of opposite charge stay during the whole simulation period. The mutual residence time between cations and anions is the longest time constant with a value of 9990 ps. It would be tempting to associate this long time constant

or the "steady-state" value $n_\infty$ with the existence of ion pairs. The respective amplitudes of 5.41 and 2.05, however, are far beyond a 1:1 ion pair. In other words, we have a long lived ion cage but not an ion pair.

Remarkably, the time constants of the $k = 2$ and $k = 3$-component for cation-cation, cation-anion and anion-anion look very similar to the time constants gained from the $\langle \mathbf{J}(0) \cdot \mathbf{J}(t) \rangle$ fit. This coincidence stresses that the translational processes responsible for the collective current can be retrieved in the cage relaxations which are representative for a local environment. In other words, although being a collective property, the current $\mathbf{J}(t)$ and hence the conductivity $\sigma(0)$ are determined by a local environment. However, this statement makes also clear, that a correct description of the interaction between a molecule and its local environment is crucial to gain reliable results for the conductivity. Therefore, the polarizability which model the reaction of a molecule to its environment should be an intrinsic part of molecular dynamics simulations of ionic liquids.

## C Collective dipolar displacement

The analysis of the cage dynamics revealed slow processes beyond the scope of the current correlation function $\langle \mathbf{J}(0) \cdot \mathbf{J}(t) \rangle$. In principle, these slow processes must show up in the collective translational properties. As explained in the Theory section, the collective dipolar displacement $\left\langle \Delta M_j^2(t) \right\rangle$ is more sensitive to these slow translational processes. Fig. 6 shows both, the numerical data of $\left\langle \Delta M_j^2(t) \right\rangle$ as well as the corresponding fit. In order to elucidate the short time behavior an inset covering the first 120 picoseconds is given, too. The fit function $f_{\Delta \mathrm{MJ}}{}^2(t)$ (orange dashed line) is multi-exponential plus an asymptotic linear part. The corresponding fit parameters are given in Table I. The first two time constants $\tau_{1+2}$ and $\tau_3$ are similar to 0.24 ps and 2.6 ps found in a dielectric study of Asaki et al.[68]

As expected from Eq. (17), the time constants $k = 1 \ldots 3$ of $\langle \mathbf{J}(0) \cdot \mathbf{J}(t) \rangle$ are also found in the collective dipolar displacement $\left\langle \Delta M_j^2(t) \right\rangle$. Since oscillations are difficult to detect in a mean-squared displacement, only the superposition of $k = 1$ and $k = 2$ is found. Furthermore, a relaxation constant $\boldsymbol{\tau}_4$ of 60.8 ps appears which agrees very well with the ~ 60 ps detected in the cage relaxation processes and lies in the range of time constants suspected from the $\sigma_{\mathrm{J}}(t)$ fit. A possible explanation for the invisibility of this process in $\langle \mathbf{J}(0) \cdot \mathbf{J}(t) \rangle$ is the down-scaling of the amplitude $A_k = \tilde{A}_k / 2\boldsymbol{\tau}_k$. For slow processes, i.e. for high values of $\boldsymbol{\tau}$ the amplitude is suppressed and hardly visible in the current correlation function. The "theoretical" values of the amplitude $A_k$ are given in brackets in Table I. The ratio between $A_{1+2}$ = -3306 $e^2$ $A^2$ $ps^{-2}$ and $A_4$ = -0.141 $e^2$ $A^2$ $ps^{-2}$ is so large, that the slow process $k = 4$ is masked by the statistical noise of $\langle \mathbf{J}(0) \cdot \mathbf{J}(t) \rangle$. Although playing a different role for slow and fast translational processes the dipolar displacement and the current correlation function must match at an intermediate level. In fact, if one integrates $\langle \mathbf{J}(0) \cdot \mathbf{J}(t) \rangle$ to get $\sigma_{\mathrm{J}}(t)$ (see Eq. (12)) or differentiates $\left\langle \Delta M_j^2(t) \right\rangle$ (see Eq. (16)) the consistency of the two completely different fits of $\langle \mathbf{J}(0) \cdot \mathbf{J}(t) \rangle$ and $\left\langle \Delta M_j^2(t) \right\rangle$ can be checked. Fig. 7 presents the result of this consistency check. The numerical integration of $\langle \mathbf{J}(0) \cdot \mathbf{J}(t) \rangle$ is again shown as gray solid

line. The fits of $\langle \mathbf{J}(0) \cdot \mathbf{J}(t) \rangle$ according to $f_{\mathrm{JJ}}(t)$ and of $\left\langle \Delta M_j^2(t) \right\rangle$ according to $f_{\Delta \mathrm{MJ}}{}^2(t)$ are represented as black dotted and orange dashed line, respectively. Except for very short times below 0.5 ps the agreement is fairly good. The deviation at very short times stems from the oscillatory behavior at short times which cannot be represented by the multi-exponential function $f_{\Delta \mathrm{MJ}}{}^2(t)$. The final value of $\sigma_{\mathrm{J}}(\tau)$ are given by Eq. (23) in case of the current correlation function and $\sigma$ in case of $\left\langle \Delta M_j^2(t) \right\rangle$ after all exponential processes have decayed. From the slope of the linear region (t > 400 ps) of $\left\langle \Delta M_j^2(t) \right\rangle$ one may get a static conductivity $\sigma(0)$ value of 0.16 S/m which is a little bit less than the value of 0.17 S/m gained from the current correlation function if one adds the $k = 4$-component of $\left\langle \Delta M_j^2(t) \right\rangle$. Based on the Nernst-Einstein equation (1) this corresponds to a collectivity factor Δ of 0.17.

## D Dielectric spectrum

In Fig. 7 we have demonstrated the agreement of the two independent fits of $\langle \mathbf{J}(0) \cdot \mathbf{J}(t) \rangle$ and $\left\langle \Delta M_j^2(t) \right\rangle$ in the time domain. The close correspondence in frequency space is illustrated in Fig. 8 for the translational part of the dielectric spectrum $\vartheta_0(\omega)$. In the high frequency range between 1 and 50 THz the two oscillatory components of the current (black dashed and dotted line) contribute two distinct peaks while the single exponent of the dipolar displacement appears as a single broad peak (orange dash-dotted line). Nevertheless, this single broad peak approximates sum of the two current peaks quite well. Although being the major player for the shape of $\langle \mathbf{J}(0) \cdot \mathbf{J}(t) \rangle$, the contribution of the first component $k = 1$ is quite less important for the spectrum of the dielectric conductivity $\vartheta_0(\omega)$. One way of explanation would be that the $k = 1$-component mainly characterizes the static conductivity $\sigma(0)$ which is subtracted from $\sigma(\omega)$ in the computation of $\vartheta_0(\omega)$. Therefore, major parts of the $k = 1$-component are not part of $\vartheta_0(\omega)$ any more and the contribution to the static value of the dielectric conductivity shrinks to 0.04. Nevertheless, the frequency $\omega_1$ is still visible in the spectrum by the crossing of the ω-axis at 17.7 THz. The negative values above 17.7 THz show that the contribution of the $k = 1$-component counteracts the contribution from $k = 2$ at these frequencies. The non-oscillatory character of the $k = 2$-component manifests in a approximately Lorentzian-shaped peak (black dotted line) in the dielectric spectrum and contributes to $\vartheta_0(0)$ with a value of 0.81 which is 20 times higher than the first component. In $\langle \mathbf{J}(0) \cdot \mathbf{J}(t) \rangle$ the $k = 2$-component decreased the static conductivity and was attributed to ion cage effects which are still present in the dielectric spectrum after the subtraction of the static conductivity. The third component of $\langle \mathbf{J}(0) \cdot \mathbf{J}(t) \rangle$ -fit (black solid line) with a time constant of $\tau_3$ =3.52 ps contributes slightly more to $\vartheta_0(0)$ with a value of 1.13. As can be already seen in Table I the $k = 3$-component gained from the collective dipolar displacement is almost identical to that of the $\langle \mathbf{J}(0) \cdot \mathbf{J}(t) \rangle$ -fit. Consequently, the respective peaks at ~ 0.3 THz coincide and their contribution to $\vartheta_0(0)$ is of equal weight. The major contribution to the dielectric conductivity spectrum $\vartheta_0(\omega)$ stems from the slowest detectable process ($k = 4$) of the collective dipolar displacement and is located at ~ 0.02 THz. Converting this peak by Kramers-Kronig to a contribution to the static dielectric conductivity yields a value of roughly 4 which is two-thirds of the total $\vartheta_0(0)$. The sum of all contributions to $\vartheta_0(0)$ is slightly higher than the value approximated in Ref. 26.

Up to now, we have discussed the translational part of the dielectric spectrum. In order to compute the spectrum of the generalized dielectric constant $\Sigma_0(\omega)$ one needs the dielectric permittivity $\epsilon(\omega)$ as well. $\epsilon(\omega)$ may be gained by Fourier-Laplace transform of a fit of $\langle \mathbf{M}_D(0)\cdot\mathbf{M}_D(t)\rangle$ according to Eq. (8) and is shown in Fig. 9 as solid black line. It may be decomposed into contributions from the cations (dotted black line) and anion (dashed black line) and their cross-term (not shown). Since the translational processes could be explained on a local level of an ion with its cage, one is tempted to apply a similar procedure[40,69] for the rotational correlation of the dipole moments. The straightforward way to find out the influence of collectivity would be the approximation of dipolar relaxation by the sum over the individual auto-correlation functions of the molecular dipole moments. For the cations (orange dotted line) and anions (orange dashed line) these single-particle correlation functions are shown in Fig. 9. Their shift to lower frequencies as compared to their collective analogues is striking, particularly for the anions. In other words, the coupling between molecular dipole moments speeds up rotational dipole relaxation. Thereby, the term “rotational” comprises all non-translational contributions. In particular, it contains the contributions from the induced dipoles mimicking the electronic response to the local environment.

The discrepancy between the corresponding black and orange curves clearly demonstrates the impact of collectivity. A measure of this collectivity in rotational relaxation is the Kirkwood $G_K$-factor

$$G_K = \frac{\mathbf{M}_D^2}{N\langle \mu^2 \rangle} \tag{24}$$

originally developed for neutral molecular liquids. [70–72] Applying this relation separately to cations and anions we find values of $G_K^+ = 0.58$ and $G_K^- = 0.65$. This indicates that the dipoles of like charges seem to prefer an overall anti parallel alignment which quenches the collective dipole moment as compared to the sum of individual dipoles. From the theory of Kivelson and Madden one would expect that collective and single particle rotational relaxation times scale with the corresponding $G_K$-factors.[71,72] Values below unity are indicative of a speed up of collective rotation as compared to single particle rotation. For the present case the acceleration is even faster showing the high cooperativeness of the molecular ions.

Altogether, the dielectric permittivity $\epsilon(\omega)$ (black dotted line) and the dielectric conductivity $\vartheta_0(\omega)$ (black dashed line) sum up to the generalized dielectric constant $\sum_0(\omega)$ (black dash-dotted line) shown in Fig. 10. It is important to note that the central peak of $\sum_0(\omega)$ can be neither attributed solely to $\epsilon(\omega)$ nor to $\vartheta_0(\omega)$. In fact, it results from the superposition of both part of the spectrum which strongly overlap. The good agreement between the computational and the experimental spectrum (gray line in Fig. 10) of Ref. 46 provides strong evidence that the findings and conclusions made so far are representative of the experimental situation. We state that this consensus between simulation and experiments depends on the inclusion of the slow process detected in the dipolar displacement. This demonstrates once more that the translational part of the dielectric spectrum of molecular

ionic liquids cannot be computed solely from the current correlation function. Rather, the combination with the dipolar displacement is essential in order to detect slow processes. Therefore, we have used the motional parameters from the current correlation function augmented by the slow process (k = 4) from $\left\langle \Delta M_j^2(t) \right\rangle$.

## V Conclusion

The dielectric behaviour of the molecular ionic liquids $EMIM^+CF_3SO_3^-$ can be neither derived from single-particle motion nor from the motional coupling of ion pairs. In fact, it is intrinsically collective. However, there is a difference between translational and rotational (including induced and vibrational) contributions:

In case of translational processes the inclusion of the ion cage accounts already for the translational cooperativeness. Thereby, the ion cage is rather heterogeneous: On average the cage is build up from eight counter ions. But also contains ten $EMIM^+$ or four $CF_3SO_3^-$ in case of a central $EMIM^+$ or $CF_3SO_3^-$, respectively. All time constants found in $\langle \mathbf{J}(0) \cdot \mathbf{J}(t) \rangle$ and $\left\langle \Delta M_j^2(t) \right\rangle$ are also present in the residence correlation functions $\left\langle n_i^j(0) \cdot n_i^j(t) \right\rangle$ around the cations and anions.

However, collective rotation involves the complete set of interacting dipoles. An approximation in single-particle terms would result in a dielectric spectrum differing substantially from experiment. This demonstrates the long-range coupling of dipolar rotation which also manifests in Kirkwood $G_K$-factor below unity for cations and anions.

Traditionally, the collective dipolar displacement $\left\langle \Delta M_j^2(t) \right\rangle$ is only used to compute the static conductivity $\sigma(0)$ from the linear region of this function. In this work we showed that the initial nonlinear region is essential for the determination of slow translational processes which contribute significantly to the dielectric spectrum at lower frequency. Furthermore, the agreement between the information gained from the current correlation function $\langle \mathbf{J}(0) \cdot \mathbf{J}(t) \rangle$ and the collective dipolar displacement $\langle \mathbf{M}_J(0) \cdot \mathbf{M}_J(t) \rangle$ for the high frequency part of the generalized dielectric constant $\sum_0^*(\omega)$ is demonstrated. The combination of these information brings one into the position to compute a dielectric spectrum which agrees well with the experimental one.

## Acknowledgments

The computational work was performed on the “Vienna Scientific Cluster” (www.zid.tuwien.ac.at/vsc) of the University of Vienna, the Vienna University of Technology, and the University of Natural Resources and Applied Life Science Vienna. We thank for generous allocation of computer time. This work was supported by Project No. P23494 of the FWF Austrian Science Fund.

## References

1. Schröder, C, Steinhauser, O. Computational Spectroscopy:Methods, Experiments and Applications. Grunenberg, J, editor. Wiley-VCH; Weinheim: 2010.
2. Weingärtner H. Angew Chem Int Ed. 2008; 47 654
3. Forsyth SA, Pringle JM, MacFarlane DR. Aust J Chem. 2004; 57 113

4. Keblinski P, Eggebrecht J, Wolf D, Phillpot SR. J Chem Phys. 2000; 113 282
5. Del Pópolo MG, Voth GA. J Phys Chem B. 2004; 108 1744
6. Bhargava BL, Klein ML, Balasubramanian S. Chem Phys Chem. 2008; 9 67 [PubMed: 18098251]
7. Xiao D, Hines LG Jr, Li S, Bartsch RA, Quitevis EL, Russina O, Triolo A. J Phys Chem B. 2009; 113 6426 [PubMed: 19358548]
8. Hardacre C, Holbrey JD, McMath SEJ, Bowron DT, Soper K. J Chem Phys. 2003; 118 273
9. Morrow TI, Maginn EJ. J Phys Chem B. 2002; 106 12807
10. Shah JK, Brennecke JF, Maginn EJ. Green Chem. 2002; 4 112
11. Liu Z, Huang S, Wang W. J Phys Chem B. 2004; 108 12978
12. Schröder C, Rudas T, Steinhauser O. J Chem Phys. 2006; 125 244506 [PubMed: 17199354]
13. MacFarlane DR, Golding J, Forsyth S, Forsyth M, Deacon GB. Chem Commun. 2001. 1430
14. Huddleston JG, Visser AE, Reichert WM, Willauer HD, Broker GA, Rogers RD. Green Chem. 2001; 3 156
15. Malvaldi M, Chiappe C. J Phys Condens Matter. 2008; 20 035108
16. Schröder C, Haberler M, Steinhauser O. J Chem Phys. 2008; 128 134501 [PubMed: 18397071]
17. Schröder C, Steinhauser O. J Chem Phys. 2008; 128 224503 [PubMed: 18554025]
18. Schröder C, Hunger J, Stoppa A, Buchner R, Steinhauser O. J Chem Phys. 2008; 129 184501 [PubMed: 19045408]
19. Shim Y, Kim HJ. J Phys Chem B. 2008; 112 11028 [PubMed: 18693693]
20. Schröder C, Steinhauser O. J. Chem. Phys. 2009; 131 114504 [PubMed: 19778126]
21. Schröder C, Steinhauser O. J Chem Phys. 2010; 132 244109 [PubMed: 20590183]
22. Schröder C, Wakai C, Weingoartner H, Steinhauser O. J Chem Phys. 2007; 126 084511 [PubMed: 17343462]
23. Caillol JM, Levesque D, Weis JJ. J Chem Phys. 1989; 91 5544
24. Caillol J-M. J Chem Phys. 1994; 101 6080
25. Borodin O. J Phys Chem B. 2009; 113 11463 [PubMed: 19637900]
26. Schröder C, Steinhauser O. J Chem Phys. 2010; 133 154511 [PubMed: 20969407]
27. Yan T, Wang Y, Knox C. J Phys Chem B. 2010; 114 6886 [PubMed: 20443608]
28. Moore, WJ, Hummel, DO, Trafara, G, Holland-Moritz, K. Physikalische Chemie. 4th ed. Walter de Gruyter; Berlin, New York: 1986.
29. Debye P, Huckel E. Physik Z. 1923; 24 185
30. McQuarrie, DA. Statistical mechanics. Harper and Row; New York, Evanston, San Fran-scisco, London: 1976.
31. Song X. J Chem Phys. 2009; 131 044503 [PubMed: 19655890]
32. Aurenhammer F. ACM Computing Surveys. 1991; 23 345
33. Okabe, A. Spatial tesselations: Concepts and applications of Voronoi diagrams. Wiley; New York: 2000.
34. Schröder C, Neumayr G, Steinhauser O. J Chem Phys. 2009; 130 194503 [PubMed: 19466839]
35. Neumayr G, Schröder C, Steinhauser O. J Chem Phys. 2009; 131 174509 [PubMed: 19895027]
36. Del Pópolo MG, Lynden-Bell RM, Kohanoff J. J Phys Chem B. 2005; 109 5895 [PubMed: 16851642]
37. Bhargava BL, Balasubramanian S. Chem Phys Lett. 2006; 417 486
38. Kirchner B, Seitsonen AP. Inorg Chem. 2007; 46 2751 [PubMed: 17330971]
39. Spickermann C, Thar J, Lehmann SBC, Zahn S, Hunger J, Buchner R, Hunt PA, Welton T, Kirchner B. J Chem Phys. 2008; 129 104505 [PubMed: 19044922]
40. Krekeler C, Dommert F, Schmidt J, Zhao YY, Holm C, Berger R, delle Site L. Phys Chem Chem Phys. 2010; 12 1817 [PubMed: 20145847]
41. Yu H, van Gunsteren WF. Comput Phys Commun. 2005; 172 69
42. Lopes PEM, Roux B, MacKerell AD Jr. Theor Chem Acc. 2009; 124 11 [PubMed: 20577578]
43. Yan T, Burnham CJ, Del Pópolo MG, Voth GA. J Phys Chem B. 2004; 108 11877

44. Smith GD, Borodin O, Li L, Kim H, Liu Q, Bara JE, gin DL, Nobel R. Phys Chem Chem Phys. 2008; 10 6301 [PubMed: 18936854]
45. Jiang W, Yan T, Wang Y, Voth GA. J Phys Chem B. 2008; 112 3121 [PubMed: 18288833]
46. Schröder C, Sonnleitner T, Buchner R, Steinhauser O. Phys Chem Chem Phys. 2011.
47. Canongia Lopes JN, Deschamps J, Padua AAH. J Phys Chem B. 2004; 108 2038
48. Canongia Lopes JN, Deschamps J, Padua AAH. J Phys Chem B. 2004; 108 11250
49. Canongia Lopes JN, Padua AAH. J Phys Chem B. 2004; 108 16893
50. Hanke CG, Price SL, Lynden-Bell RM. Mol Phys. 2001; 99 801
51. Anisimov VM, Lamoureux G, Vorobyov IV, Huang N, Roux B, MacKerell AD. J Chem Theory Comput. 2005; 1 153 [PubMed: 26641126]
52. Harder E, Anisimov VM, Whitfield T, MacKerell AD Jr, Roux B. J Phys Chem B. 2008; 112 3509 [PubMed: 18302362]
53. van Duijnen PT, Swart M. J Phys Chem A. 1998; 102 2399
54. Harder E, Anisimov VM, Vorobyov IV, Lopes PEM, Noskov SY, MacKerell AD Jr, Roux B. J Chem Theory and Comp. 2006; 2 1587
55. Lamoureux G, Roux B. J Chem Phys. 2003; 119 3025
56. Darden T, York D, Pedersen L. J Chem Phys. 1993; 98 10089
57. Essmann U, Perera L, Berkowitz ML, Darden T, Lee H, Pedersen LG. J Chem Phys. 1995; 103 8577
58. Neumann M, Steinhauser O. Chem Phys Lett. 1984; 106 563
59. Salanne M, Simon C, Turq P, Madden PA. J Phys Chem B. 2007; 111 4678 [PubMed: 17388450]
60. Siqueira LJA, Ribeiro MCC. J Phys Chem B. 2007; 111 11776 [PubMed: 17877389]
61. Pićalek J, Kolafa J. J Mol Liquids. 2007; 134 29
62. Bhargava BL, Balasubramanian S. J Chem Phys. 2005; 123 144505 [PubMed: 16238405]
63. Rey-Castro C, Vega LF. J Phys Chem B. 2006; 110 14426 [PubMed: 16854152]
64. Kowsari MH, Alavi S, Ashrafizaadeh M, Najafi B. J Chem Phys. 2009; 130 014703 [PubMed: 19140627]
65. Wulf A, Fumino K, Ludwig R. Angew Chem Int Ed. 2010; 49 449
66. Wulf A, Fumino K, Ludwig R, Taday PF. Chem Phys Chem. 2010; 11 349 [PubMed: 19967732]
67. English NJ, Mooney DA, O'Brien SW. J Mol Liquids. 2010; 157 163
68. Asaki MLT, Redondo A, Zawodzinski TA, Taylor AJ. J Chem Phys. 2002; 116 10377
69. Koßmann S, Thar J, Kirchner B, Hunt PA, Welton T. J Chem Phys. 2006; 124 174506 [PubMed: 16689582]
70. Kirkwöd JG. J Chem Phys. 1939; 7 911
71. Boottcher, CJF, Bordewijk, P. Theory of electric polarization. Vol. 1. Elsevier; Amsterdam: 1978.
72. Madden P, Kivelson D. Adv Chem Phys. 1984; 56 467


Europe PMC Funders Author Manuscripts

Europe PMC Funders Author Manuscripts

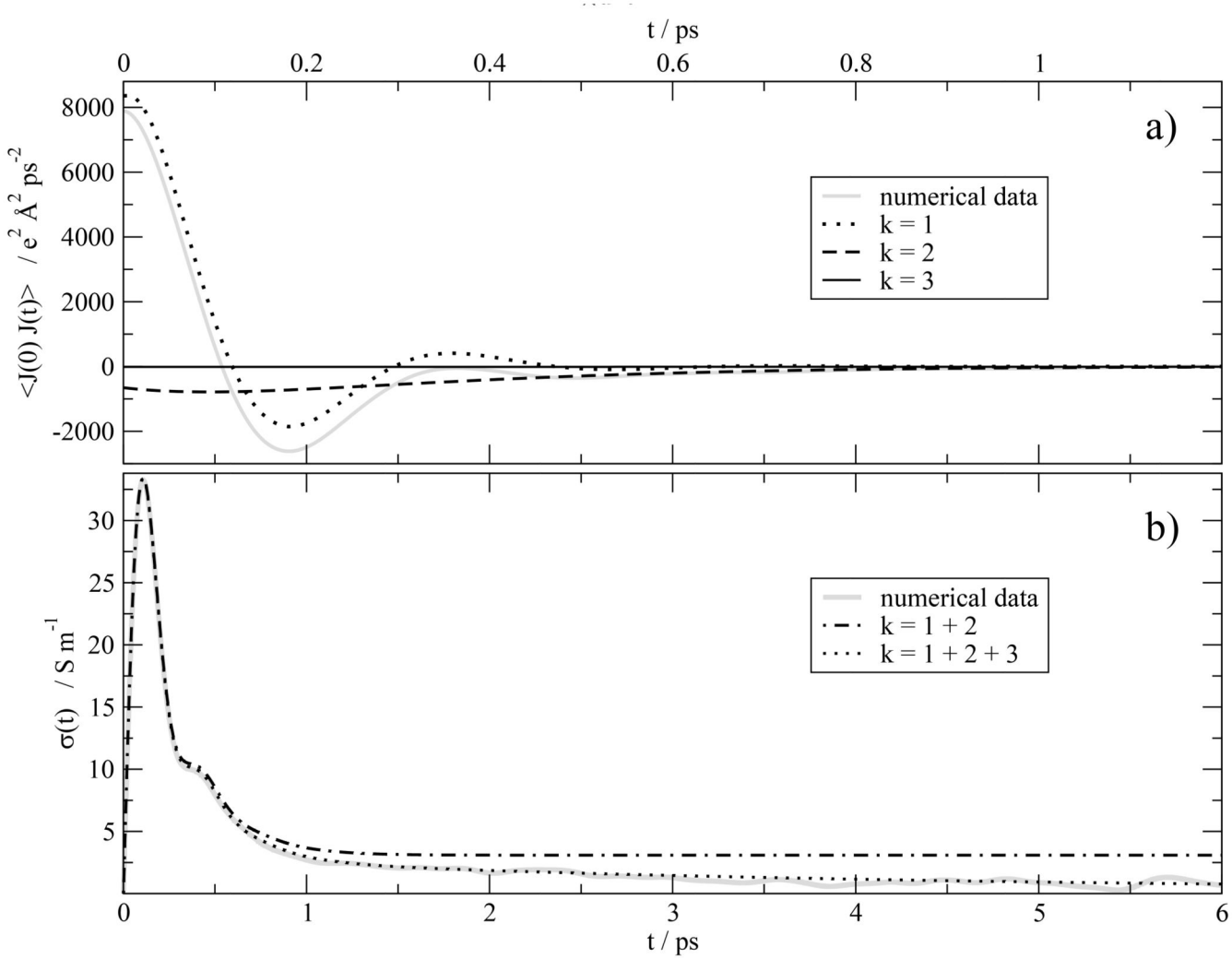


**Fig. 1.**

a) Auto-correlation function of the current $\mathbf{J}(t)$ and its decomposition into its components $k = 1 \ldots 3$. (b) The importance of the $k = 3$-contribution becomes visible in $\sigma_J(t)$ which is the running integral of $\langle \mathbf{J}(0) \cdot \mathbf{J}(t) \rangle$.

Europe PMC Funders Author Manuscripts

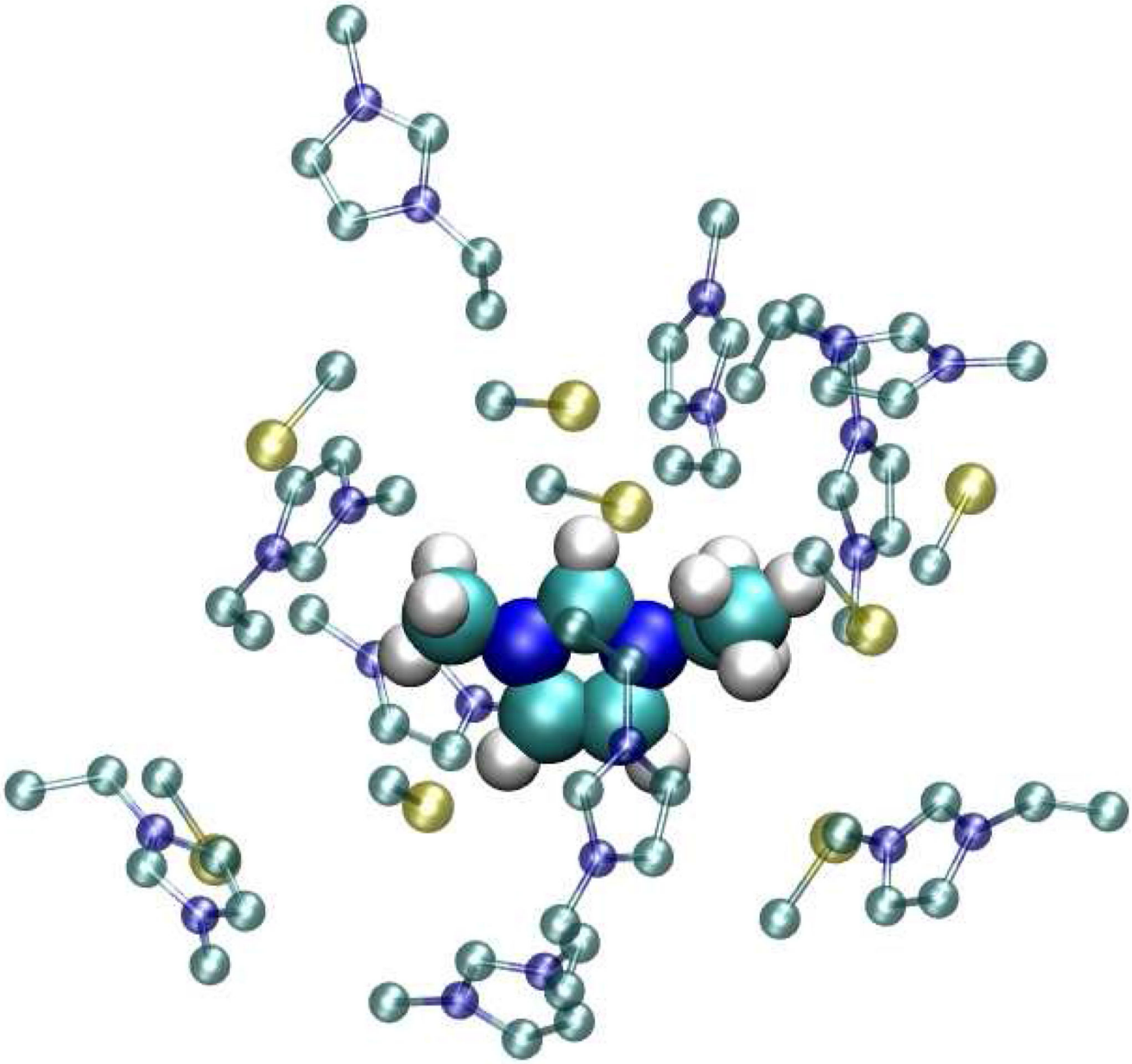

**Fig. 2.**

A snapshot of first shell members of 1-ethyl-3-methyl-imidazolium. For the sake of simplicity the hydrogens of the surrounding imidazoliums and the fluorines and oxygens of triflate are not displayed.

Europe PMC Funders Author Manuscripts

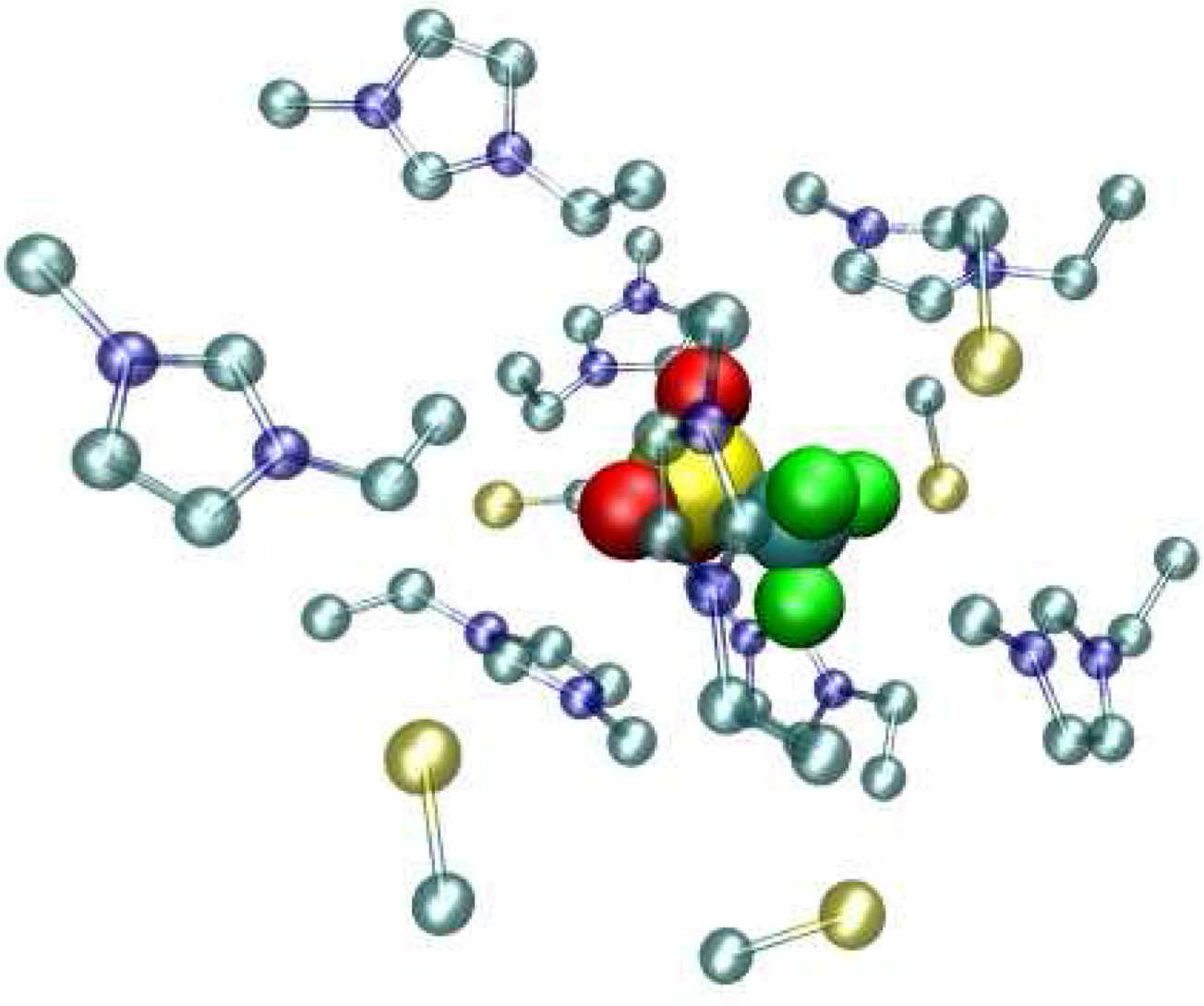

**Fig. 3.**

A snapshot of first shell members of triflate. For the sake of simplicity the hydrogens of the surrounding imidazoliums and the fluorines and oxygens of triflate are not displayed.

Europe PMC Funders Author Manuscripts

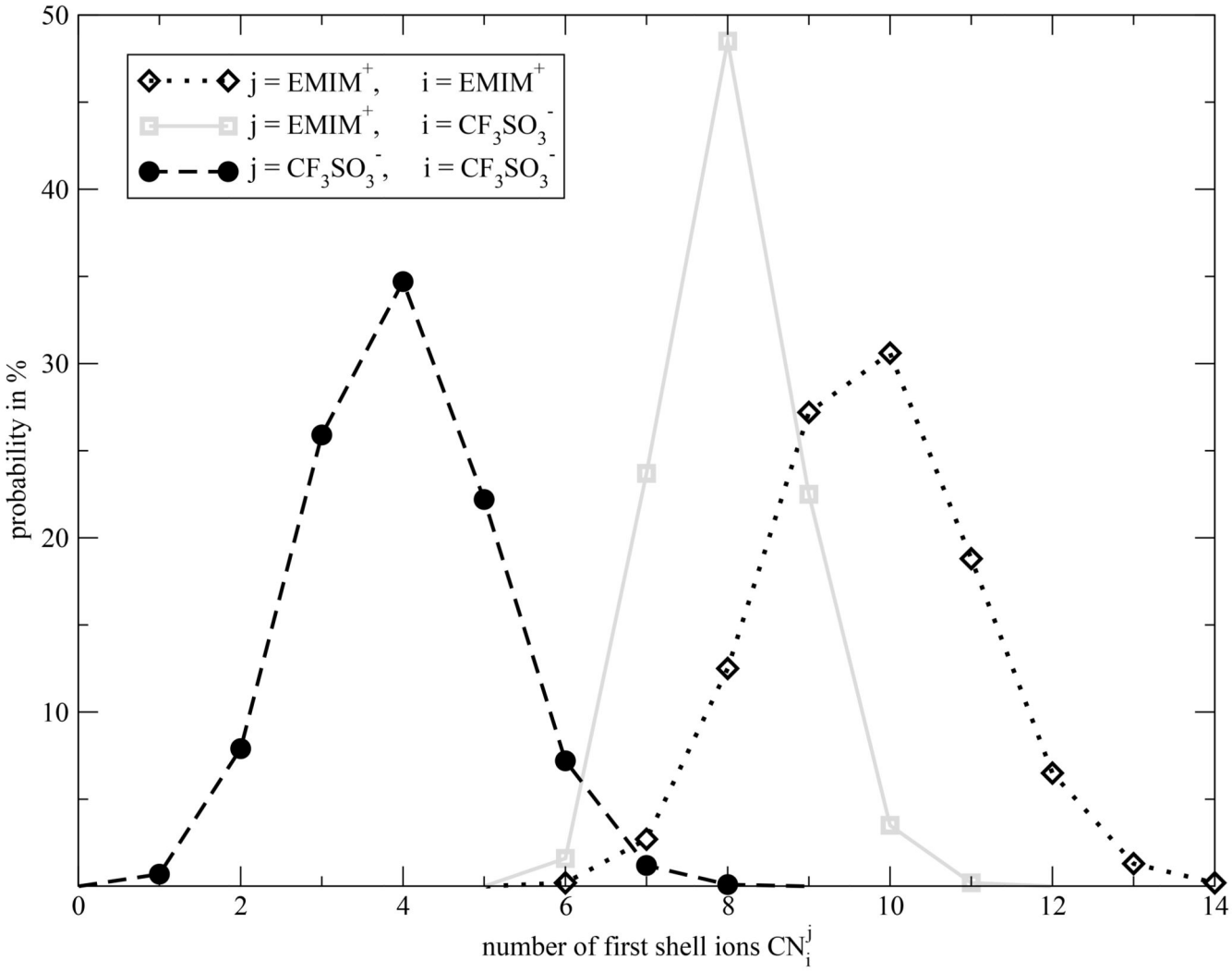


**Fig. 4.**

Distribution of mutual coordination numbers. *j* denotes the central ion species and *i* the surrounding species.

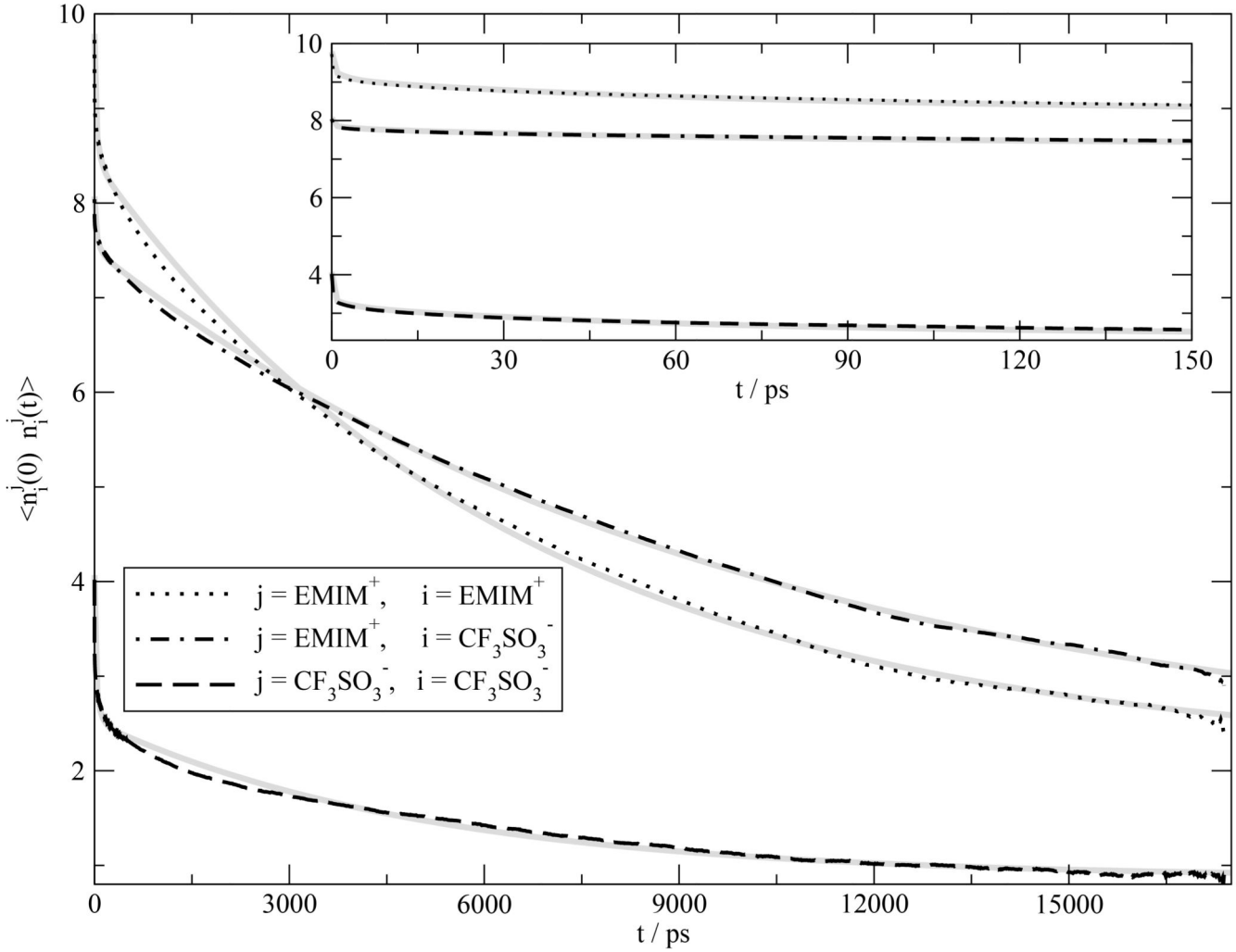


**Fig. 5.**

Mutual mean residence function $C_i^j(t)$. $j$ denotes the central ion species and $i$ the surrounding species (black curves). The inset represents the first 150 picoseconds. All curves can be fitted according to $f_{nn}(t)$ (respective gray curves) with the parameters in Table II.

Europe PMC Funders Author Manuscripts

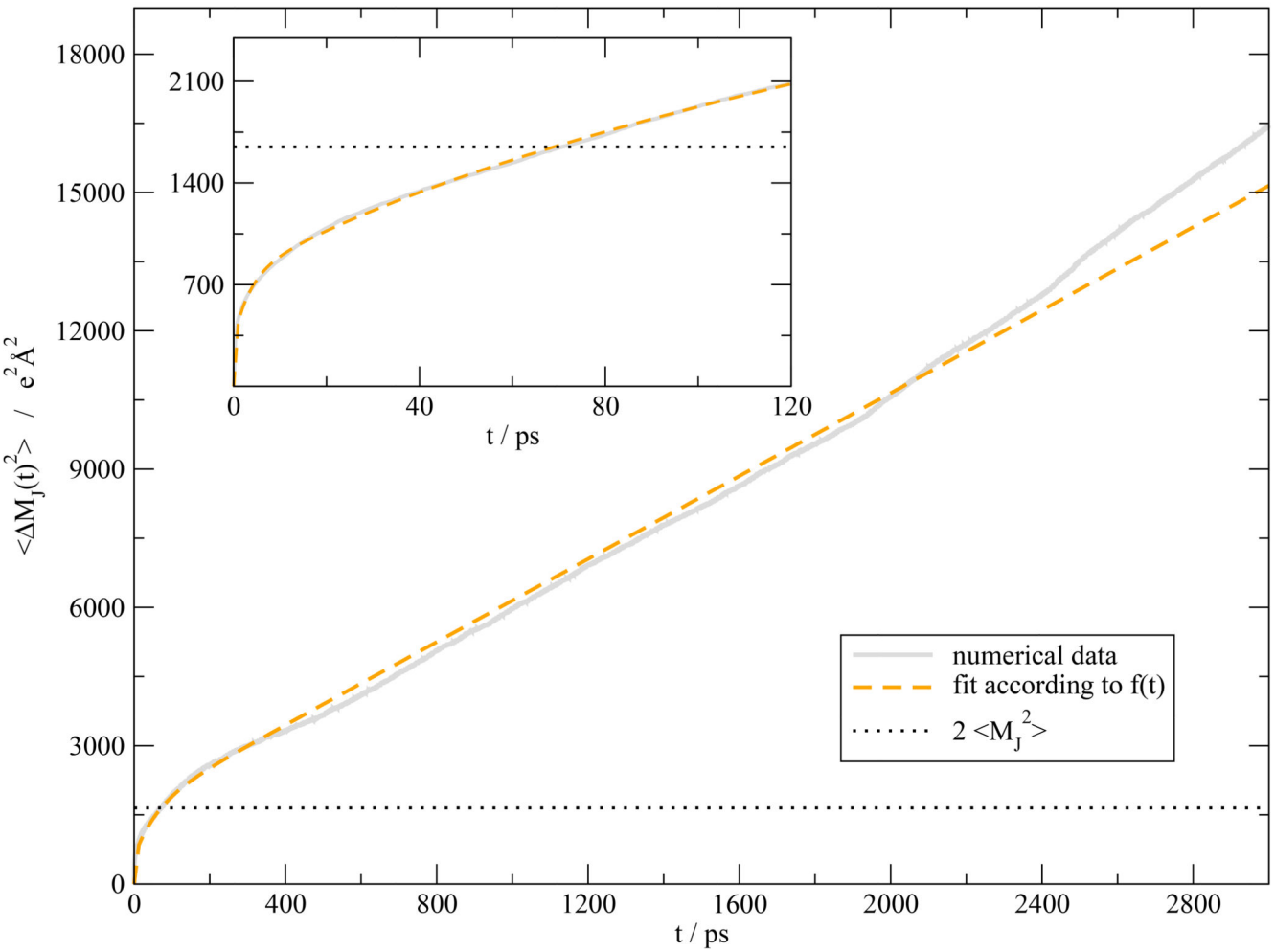


**Fig. 6.**

Mean squared-displacements of the unfolded collective rotational dipole moment $M_J(t)$. The solid gray curve is gained from the whole simulation period. The orange dashed curve represents the fit to $f_{\Delta M J}{}^2(t)$ with the values given in Table I. The inset displays the first 120 ps. As can be seen from the dotted line of $\langle \mathbf{M}_J^2 \rangle$ the inset is far away from the linear regime.

Europe PMC Funders Author Manuscripts

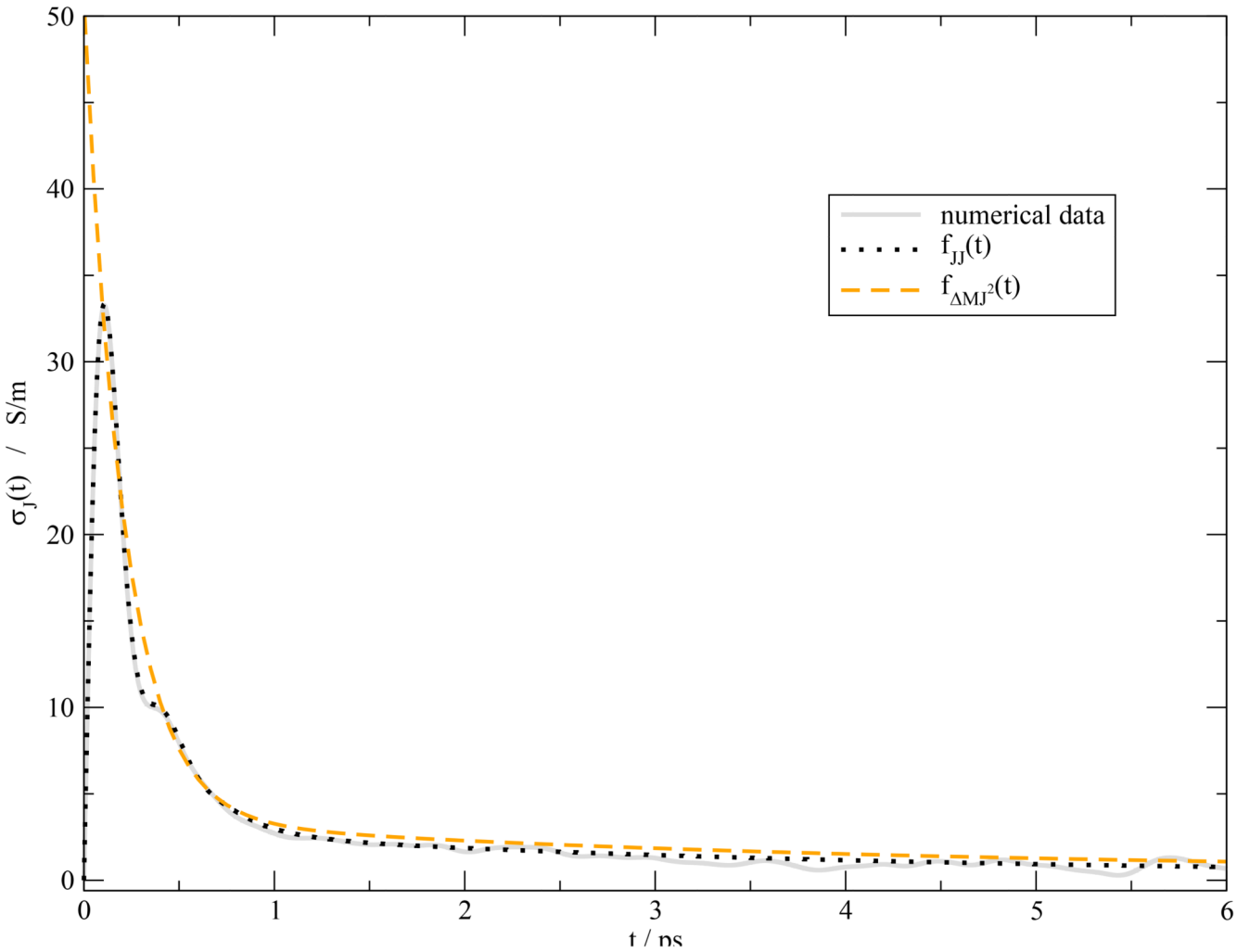


**Fig. 7.**

Running integral $\sigma_J(t)$. The gray line represents the numerical integration of $\langle \mathbf{J}(0) \cdot \mathbf{J}(t) \rangle$. The black dotted line and the orange dashed line display the fit $f_{JJ}(t)$ and $f_{\Delta MJ}{}^2(t)$ with the values given in Table I.

Europe PMC Funders Author Manuscripts

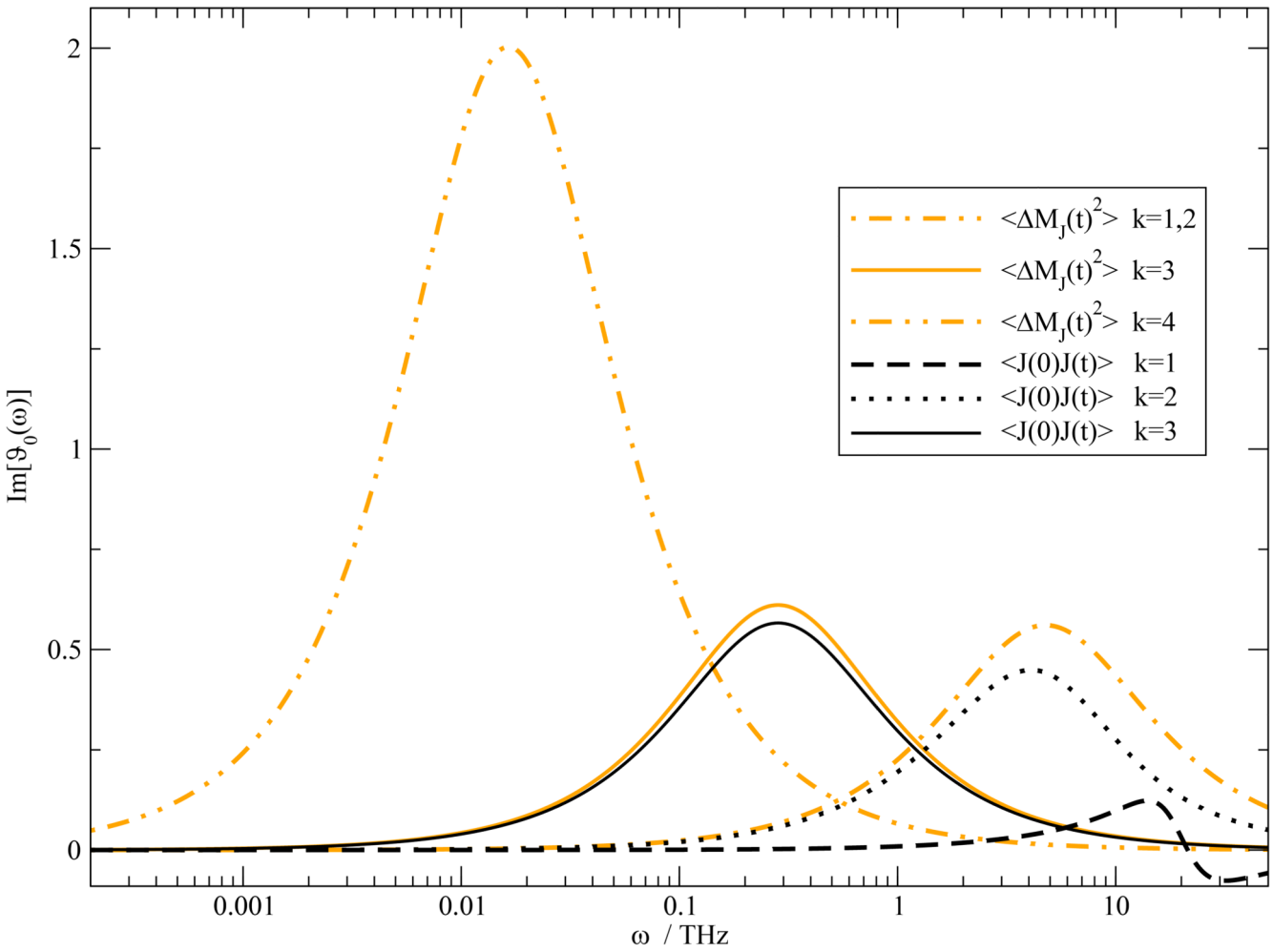


**Fig. 8.**

Juxtaposition of the individual fit components of $\langle \mathbf{J}(0) \cdot \mathbf{J}(t) \rangle$ (orange) and $\langle \mathbf{M}_J(0) \cdot \mathbf{M}_J(t) \rangle$ (black) contributing to the dielectric conductivity $\vartheta_0(\omega)$.

Europe PMC Funders Author Manuscripts

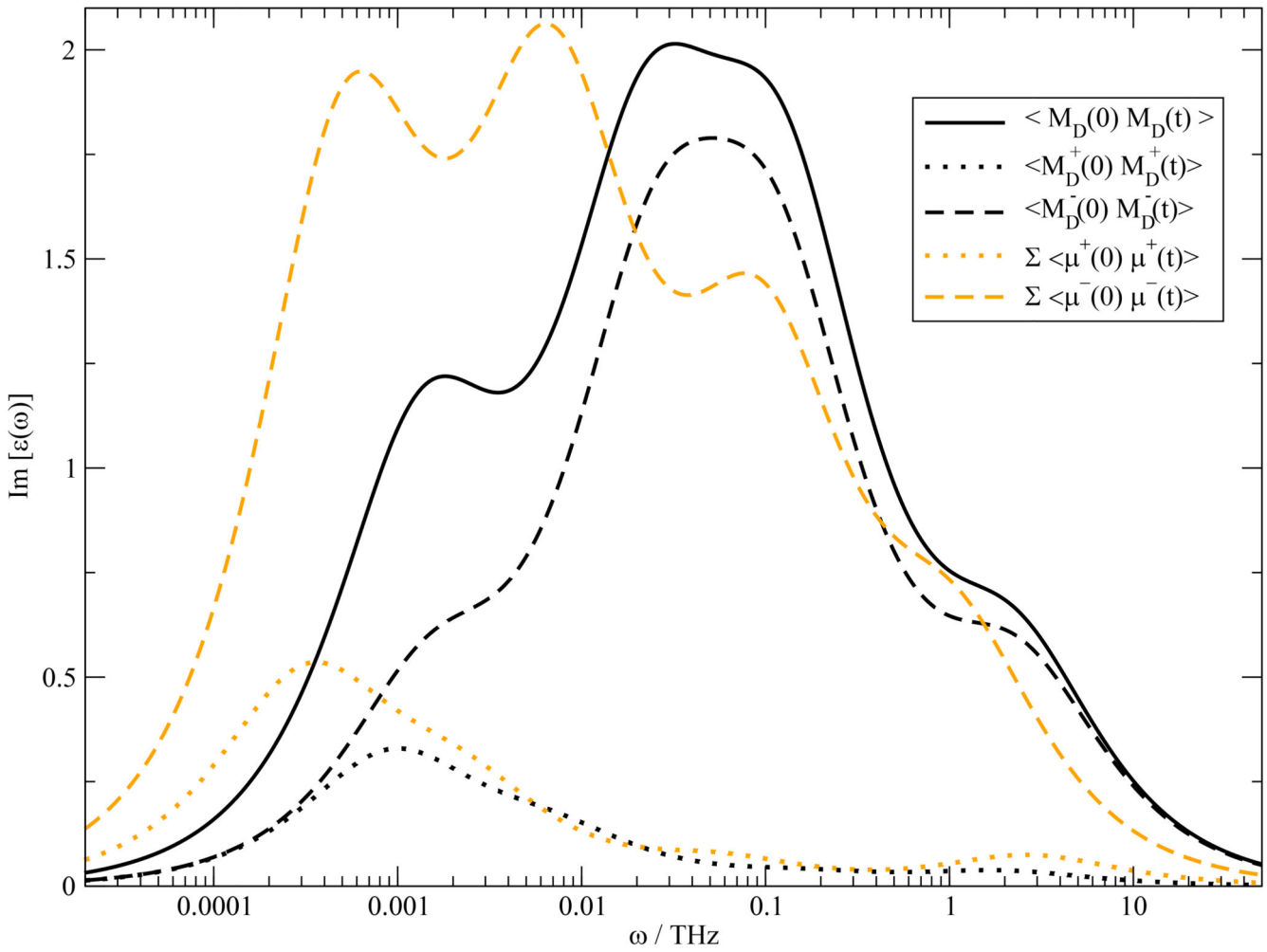


**Fig. 9.**

Imaginary part of the dielectric permittivity $\epsilon(\omega)$ (black solid line). It is built up by the cationic contribution (black dotted line), the anionic contribution (black dashed line) and the cross-term between cations and anions (not shown). If one *completely neglects collectivity*, the contribution of the cations and anions is given by the orange dotted and orange dashed line respectively.

Europe PMC Funders Author Manuscripts

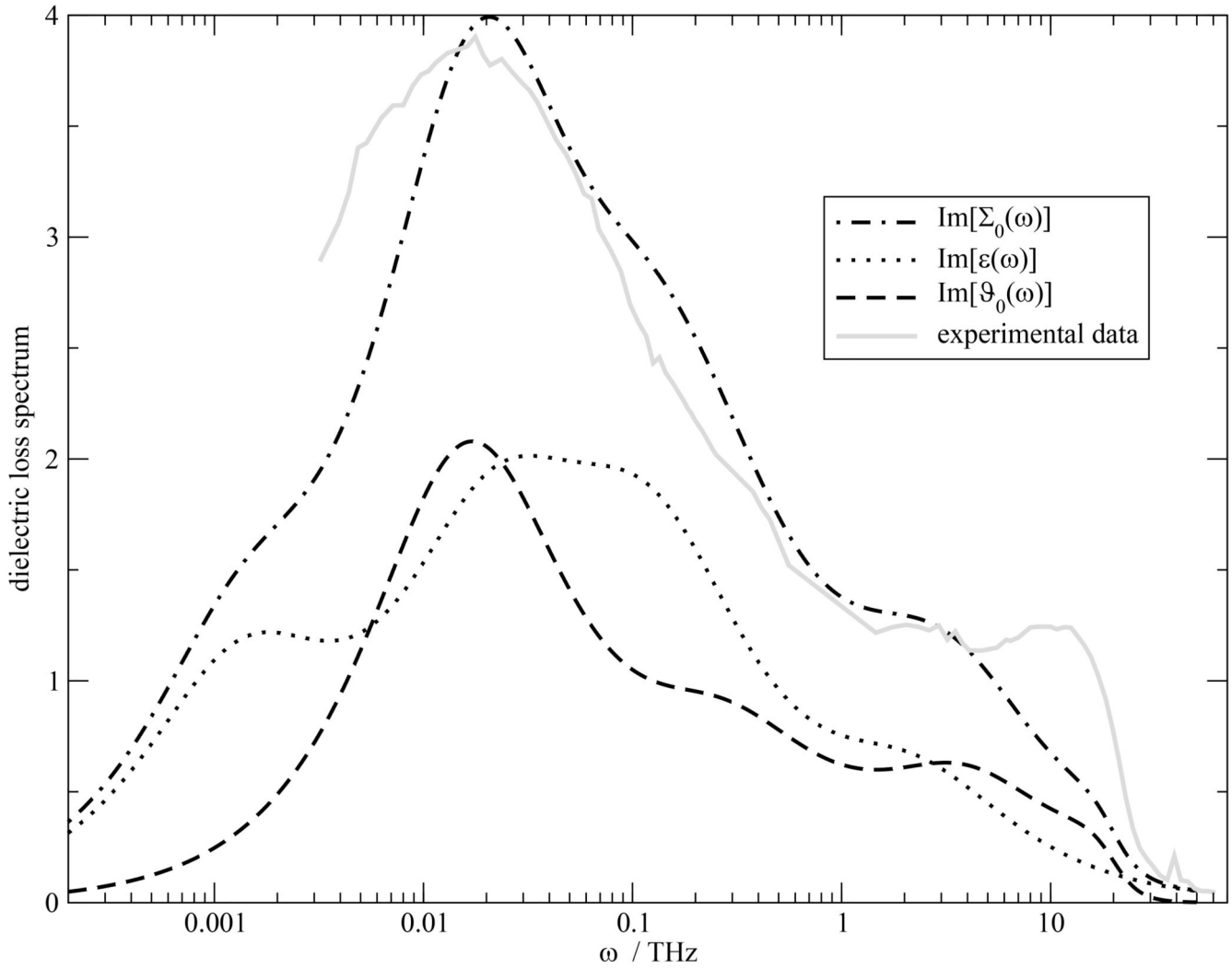


**Fig. 10.**

Dielectric loss spectrum of the generalized dielectric constant $\sum_0^*(\omega)$ (dash-dotted line). It can be decomposed into the dielectric permittivity $\epsilon(\omega)$ (dotted line) and the dielectric conductivity $\vartheta_0(\omega)$ (dashed line). For comparison the experimental spectrum is given by the gray line.[46]

Europe PMC Funders Author Manuscripts

**Table I**

The top table shows fit parameter of $\langle \mathbf{J}(0) \cdot \mathbf{J}(t) \rangle$ according $f_{\mathrm{jj}}(t)$. The bottom table shows the corresponding fit values of $\left\langle \Delta M_j^2(t) \right\rangle$ according to $f_{\Delta \mathrm{MJ}^2}(t)$. The values of $A_k$ in brackets in the bottom table are derived via $A_k = \tilde{A}_k / 2\tau_k^2$.

| $\langle \mathbf{J}(0) \cdot \mathbf{J}(t) \rangle$ | | $f_{\mathrm{JJ}}(t) = \sum_k A_k \cos(\omega_k t + \delta_k) \exp(-t/\tau_k)$ | | | |
|---|---|---|---|---|---|
| $k$ | $A_k \left[ e^2 \text{Å}^2 \text{ps}^{-2} \right]$ | $\tau_k$ [ps] | $\omega_k$ [THz] | $\delta_k$ | $\vartheta_0(0)$ |
| 1 | 9052 | 0.123 | 17.732 | -0.513 | 0.04 |
| 2 | 254800 | 0.167 | 0.04418 | 1.571 | 0.81 |
| 3 | -11.84 | 3.52 | **0.00000** | **0.000** | 1.13 |
| $\left\langle \Delta M_j^2(t) \right\rangle$ | | $f_{\Delta \mathrm{MJ}^2}(t) = \left( \sum_k \tilde{A}_k \exp(-t/\tau_k) - \tilde{A}_k \right) + \tilde{\sigma} \cdot t$ | | | |
| $k$ | $A_k \left[ e^2 \text{Å}^2 \text{ps}^{-2} \right]$ | $\tilde{A}_k \left[ e^2 \text{Å}^2 \right]$ | $\tau_k$ [ps] | $\tilde{\sigma}/6V\, k_B T$ [S/m] | $\vartheta_0(0)$ |
| 1+2 | (-3306) | -291.589 | 0.210 | 0.16 | 1.12 |
| 3 | (-12.77) | -314.655 | 3.51 | | 1.22 |
| 4 | (-0.141) | -1042.45 | 60.8 | | 4.01 |

**Table II**

**Fit parameters of the correlation of the residence function $\left\langle n_i^j(0) \cdot n_i^j(t) \right\rangle$ according to**

$$f_{\mathrm{nn}}(t) = n_\infty + \sum_k \tilde{n}_k \cdot \exp(-t/\mathcal{T}_k) .$$

| central ion *j* | surrounding ion *i* | *k* | $n_\infty$ | $\tilde{n}_k$ | $\tau_k$ / ps |
|---|---|---|---|---|---|
| $EMIM^+$ | $EMIM^+$ | | 2.15 | | |
| | | 2 | | 0.47 | 0.195 |
| | | 3 | | 0.26 | 2.85 |
| | | 4 | | 0.62 | 61.3 |
| | | 5 | | 6.29 | 6560 |
| | | $\langle\tau\rangle$ | | | 5410 |
| $EMIM^+$ | $CF_3SO_3^-$ | | 2.05 | | |
| | | 2 | | 0.19 | 0.240 |
| | | 3 | | 0.072 | 3.58 |
| | | 4 | | 0.30 | 61.2 |
| | | 5 | | 5.41 | 9990 |
| | | $\langle\tau\rangle$ | | | 9050 |
| $CF_3SO_3^-$ | $CF_3SO_3^-$ | | 0.87 | | |
| | | 2 | | 0.70 | 0.206 |
| | | 3 | | 0.19 | 3.82 |
| | | 4 | | 0.66 | 59.0 |
| | | 5 | | 1.65 | 5050 |
| | | $\langle\tau\rangle$ | | | 2610 |